Monthly Notices
of the
ROYAL ASTRONOMICAL SOCIETY

MNRAS **450,** 2393–2403 (2015) doi:10.1093/mnras/stv726

Detecting gravitational waves from mountains on neutron stars in the advanced detector era

B. Haskell,[1]★ M. Priymak,[1] A. Patruno,[2,3] M. Oppenoorth,[4] A. Melatos[1] and P. D. Lasky[1,5]

[1]*School of Physics, The University of Melbourne, Parkville, VIC 3010, Australia*
[2]*Leiden Observatory, Leiden University, PO Box 9513, NL-2300 RA Leiden, the Netherlands*
[3]*ASTRON, the Netherlands Institute for Radio Astronomy, Postbus 2, NL-7990 AA Dwingeloo, the Netherlands*
[4]*Copernicus Institute of Sustainable Development, University of Utrecht, PO Box 80.115, NL-3508 TA Utrecht, the Netherlands*
[5]*Monash Centre for Astrophysics, School of Physics and Astronomy, Monash University, VIC 3800, Australia*

Accepted 2015 March 30. Received 2015 March 26; in original form 2015 January 24

ABSTRACT

Rapidly rotating neutron stars (NSs) in low-mass X-ray binaries (LMXBs) are thought to be interesting sources of gravitational waves (GWs) for current and next generation ground-based detectors, such as Advanced LIGO and the Einstein Telescope. The main reason is that many of the NSs in these systems appear to be spinning well below their Keplerian break-up frequency, and it has been suggested that torques associated with GW emission may be setting the observed spin period. This assumption has been used extensively in the literature to assess the strength of the likely GW signal. There is now, however, a significant amount of theoretical and observation work that suggests that this may not be the case, and that GW emission is unlikely to be setting the spin equilibrium period in many systems. In this paper we take a different starting point and predict the GW signal strength for two physical mechanisms that are likely to be at work in LMXBs: crustal mountains due to thermal asymmetries and magnetically confined mountains. We find that thermal crustal mountains in transient LMXBs are unlikely to lead to detectable GW emission, while persistent systems are good candidates for detection by Advanced LIGO and by the Einstein Telescope. Detection prospects are pessimistic for the magnetic mountain case, unless the NS has a buried magnetic field of $B \approx 10^{12}$ G, well above the typically inferred exterior dipole fields of these objects. Nevertheless, if a system were to be detected by a GW observatory, cyclotron resonant scattering features in the X-ray emission could be used to distinguish between the two different scenarios.

Key words: gravitational waves – stars: neutron – X-rays: binaries.

1 INTRODUCTION

Rapidly rotating neutron stars (NSs) are considered an interesting source of gravitational waves (GWs) and are one of the main targets for current searches with ground-based detectors, such as Virgo and LIGO (Riles 2013). The characteristic amplitude of the GW signal scales with the square of the rotation frequency, thus making the more rapidly rotating NSs ideal candidates for detection. In particular some of the most promising targets are likely to be accreting NSs in low-mass X-ray binaries (LMXBs). Not only are these NSs rotating with millisecond periods, but the process of accretion from the companion star can drive the growth of a quadrupolar deformation. Plausible mechanisms that may be at work are the creation of a 'mountain' (i.e. any kind of non-axisymmetric deformation that gives rise to an $l = m = 2$ mass quadrupole) supported by the elastic crust (Bildsten 1998; Ushomirsky, Cutler & Bildsten 2000; Haskell, Jones & Andersson 2006; Johnson-McDaniel & Owen 2013) or by a solid core of exotic matter (Owen 1995; Haskell et al. 2007), unstable modes of oscillation of the star (Andersson 1998; Andersson, Kokkotas & Stergioulas 1999) and magnetically supported mountains (Cutler 2002; Melatos & Payne 2005; Haskell et al. 2008; Vigelius & Melatos 2009a; Priymak, Melatos & Payne 2011).

LMXBs were originally invoked as a source of GWs to solve an observational puzzle. In an LMXB the NS is spun up by matter accreted from the companion via a disc. This is, in fact, how old NSs are thought to be recycled to millisecond periods

★ E-mail: brynmor.haskell@unimelb.edu.au

and eventually produce a millisecond radio pulsar after accretion stops (Alpar et al. 1982; Radhakrishnan & Srinivasan 1982; Papitto et al. 2013b). One would therefore expect the NS to be spun up to its centrifugal break-up frequency, which is equation of state dependent, but generally well above 1 kHz (Cook, Shapiro & Teukolsky 1994; Haensel, Lasota & Zdunik 1999). This is not, however, what is observed. The distribution of spins in both LMXBs and millisecond radio pulsars appears to have a statistically significant cut-off at around 730 Hz (Chakrabarty et al. 2003; Patruno 2010).

It is natural to ask what physical process removes angular momentum from the NS and prevents it from spinning up further. The first and most obvious candidate is the interaction between the stellar magnetic field and the accretion disc. This possibility was examined in detail by White & Zhang (1997) who found that, at least for the data available at the time, this scenario would involve an unexpected correlation between the accretion rate and magnetic field strength (which would also need to be higher than expected). This led to the alternative suggestion that GWs may be providing the torque needed to balance the accretion torques, and set the spin equilibrium period of these systems (Papaloizou & Pringle 1978; Wagoner 1984; Bildsten 1998).

A corollary of GW torque balance is that the brightest X-ray sources should also be the loudest GW emitters (Bildsten 1998). This describes the nearby LMXB Scorpius X-1, which has been the subject of a number of LIGO and Virgo searches (Abbott et al. 2007a,b; Abadie et al. 2011; Aasi et al. 2014a) that have led to a 90 per cent confidence upper limit for the GW strain of $h_{\rm rms} \approx 10^{-25}$ around 150 Hz. With advanced detectors, such as Advanced LIGO (ALIGO), now coming online there is a strong case to develop directed data analysis algorithms (Aasi et al. 2014b) and all-sky pipelines that search for unknown binary systems (Goetz & Riles 2011).

Although GW searches with initial LIGO are still not sensitive enough to probe the predictions of the GW torque balance scenario, the problem has been recently reassessed by several authors. Patruno, Haskell & D'Angelo (2012) found that with current data the strong correlation between magnetic field and accretion rate found by White & Zhang (1997) is no longer needed and the measured spin period of most systems can be understood in terms of the disc/magnetosphere interaction (Andersson et al. 2005). Furthermore a detailed analysis of individual systems shows that many of them do, in fact, appear to be close to a propeller phase in which the spin-up torque is much weaker than in standard accretion models (Haskell & Patruno 2011; Ferrigno et al. 2013). Finally the measurements of spins and surface temperatures for most NSs in LMXBs are not consistent with theoretical predictions for GW emission due to an unstable r mode (or at least not at a level that would allow for spin equilibrium due to torque balance; Ho, Andersson & Haskell 2011; Haskell, Degenaar & Ho 2012; Mahmoodifar & Strohmayer 2013).

GW torque balance supplies a useful upper limit to calibrate searches. However if it is not the driving force behind pulsar spin evolution, it is natural to ask at what level the physical mechanisms mentioned above will give rise to GW emission, and whether it is likely to be detected. This question is crucial, given that Watts et al. (2008) showed that even at the torque balance level these systems would be challenging to detect. In this paper we explore the non-torque-balance scenario in more detail. We focus on 'mountains', supported either by elasticity or magnetic stresses, and discuss the level at which GW emission may be expected. We also take the discussion one step further and ask, given a GW detection, what constraints can be set on NS interior physics and how one could distinguish between the different mechanisms giving rise to the mountain using electromagnetic (e.g. X-ray) observations.

2 THERMAL MOUNTAINS

2.1 Crustal heating

The outer, low-density layers of an NS are thought to form a crystalline crust of ions arranged in a body-centred cubic lattice (although recent work by Kobyakov & Pethick 2014 suggests that much more inhomogeneous configurations may be possible). Above densities of $\approx 10^{11}$ g cm^{-3}, neutrons drip out of nuclei and form a superfluid in mature NSs with internal temperatures $T \lesssim 10^9$ K. At higher densities several phase transitions may occur, with nuclei no longer being spherical but forming rods and plates, the so called 'pasta' phases (Lorenz, Ravenhall & Pethick 1970), until at $\approx 2 \times 10^{14}$ g cm^{-3} there is a transition to a fluid of neutrons, protons and electrons which forms the core of the NS.

In LMXBs accreted matter, composed of light elements, is buried by accretion and compressed to higher densities, where it undergoes a series of nuclear reactions such as electron captures, neutron emission and pycnonuclear reactions (Haensel & Zdunik 1990). The observed cooling of transient LMXBs, as they enter quiescence, is consistent with a crust that has previously been heated by such reactions – see e.g. Wijnands, Degenaar & Page 2013 and references therein, although not all details of the cooling processes are fully understood (Degenaar et al. 2013; Schatz et al. 2014).

Accretion asymmetries can produce asymmetries in composition and in heating, which in turn deform the star and lead to a quadrupole (Ushomirsky et al. 2000). Once the quadruple Q_{22} is known the GW amplitude can be calculated as

$$h_0 = \frac{16}{5}\left(\frac{\pi}{3}\right)^{1/2}\frac{GQ_{22}\Omega^2}{dc^4}, \tag{1}$$

where G and c are the gravitational constant and the speed of light respectively, d is the distance to the source and Ω is the angular frequency of the star. Note that we are considering a quadrupolar Y_{22} deformation, as this harmonic dominates GW emission. In this case GWs are emitted at twice the rotation frequency of the star. An approximate expression for the quadrupole due to asymmetric crustal heating from nuclear reactions in the crust is given by (Ushomirsky et al. 2000)

$$Q_{22} \approx 1.3 \times 10^{35} R_6^4 \left(\frac{\delta T_{\rm q}}{10^5\,{\rm K}}\right)\left(\frac{Q}{30\,{\rm MeV}}\right)^3\ {\rm g\ cm^2}, \tag{2}$$

where R_6 is the stellar radius in units of 10^6 cm, $\delta T_{\rm q}$ is the *quadrupolar* component of the temperature variation due to nuclear reactions and Q is the reaction threshold energy. Higher threshold energies correspond to higher densities. In general the reactions will heat the region by an amount (Ushomirsky & Rutledge 2001)

$$\frac{\delta T}{(10^6\,K)} \approx C_k^{-1} p_d^{-1} Q_n \Delta M_{22}, \tag{3}$$

where C_k is the heat capacity per baryon in units of the Boltzman constant $k_{\rm B}$, p_d is the pressure, in units of 10^{30} erg cm^{-3}, at which the reaction occurs, Q_n is the heat per unit baryon (in MeV) deposited by the reactions and ΔM_{22} is the deposited mass in units of 10^{22} g. Note that δT in equation (3) is the total increase in temperature; only a fraction $\delta T_{\rm q}/\delta T \ll 1$ is likely to be asymmetric in general and specifically quadrupolar. Ushomirsky et al. (2000) estimate that $\delta T_{\rm q}/\delta T \leq 0.1$, but in reality the ratio is poorly known.

Table 1. LMXBs for which we have obtained an estimate of the outburst duration Δt and average accretion rate $\langle \dot{M} \rangle$. Where the reference column indicates 'this work', we have used a fiducial power-law index of $\Gamma = 2$ and the Galactic absorption column from Kalberla et al. (2005). We also list the distance d of the system and the spin frequency ν. Sources in the top half of the table are AMXPs, while those in the bottom half are NP pulsars and their frequency is inferred from the frequency of burst oscillations, as explained in the text. We do not attempt to explicitly estimate the errors associated with these measurements. The most uncertain quantity is the distance, but our main conclusions on the detectability of the GW signals are unlikely to change unless there is a substantial error in the values below.

Source	ν (Hz)	d (kpc)	$\langle \dot{M} \rangle$ ($10^{-10}\,\mathrm{M_\odot\ yr^{-1}}$)	Δt (d)	Ref.
SAX J1808.4−3658	401	3.5	4	30	Patruno et al. (2009)
XTE J1751−305	435	7.5	10	10	Miller et al. (2003)
XTE J1814−338	314	8	2	60	This work
IGR J00291+5934	599	5	6	14	Falanga et al. (2005)
HETE J1900.1−2455	377	5	8	3000	Papitto et al. (2013a)
Aql X-1	550	5	10	30	Güngör, Güver & Eksi (2014)
Swift J1756.9−2508	182.1	8	5	10	Krimm et al. (2007)
NGC 6440 X-2	204.8	8.5	1	4	This work
IGR J17511−3057	244.9	6.9	6	24	Falanga et al. (2011)
IGR J17498−2921	400.9	7.6	6	40	Falanga et al. (2012)
Swift J1749.4−2807	518	6.7	2	20	Ferrigno et al. (2011)
EXO 0748−676	552	5.9	3	8760	Degenaar et al. (2011)
4U 1608−52	620	3.6	20	700	Gierlinski & Done (2002)
KS 1731−260	526	7	11	4563	Narita, Grindlay & Barret (2001)
SAX J1750.8−2900	601	6.8	4	100	This work
4U 1636−536	581	5	30	pers.	This work
4U 1728−34	363	5	5	pers.	Egron et al. (2011)
4U 1702−429	329	5.5	23	pers.	This work
4U 0614+091	415	3.2	6	pers.	Piraino et al. (1999)

After an accretion outburst, as the system returns to quiescence, the deformations are erased on the crust's thermal time-scale (Brown, Bildsten & Rutledge 1998):

$$\tau_{\rm th} \approx 0.2\ p_d^{3/4}\ \mathrm{yr}. \quad (4)$$

If the system is in quiescence for longer than the thermal time-scale in equation (4), Q_{22} is likely to be washed out and a new mountain is rebuilt during the next outburst. A shorter recurrence time, on the other hand, could lead to an incremental accumulation of material. However, compositional asymmetries may be frozen into the crust, and not be erased on a thermal time-scale, allowing for the mountain to be built incrementally (Ushomirsky et al. 2000). This scenario predicts the formation of large quadrupoles in all transient systems ($10^{38} \lesssim Q \lesssim 10^{40}$ g cm^2), as we discuss in Section 2.4. The implied spin-down rate, in the case of four transient systems (SAX J1808.4−3658, XTE J1751−305, IGR J00291+5934 and SWIFT J1756.9−2508) is already excluded by measurements of the spin-down rate between outbursts (Patruno & Watts 2012). We do not consider this scenario further, but note that if it were to occur in any transient system, the GW strain would be comparable to that of a persistent system.

2.2 Maximum quadrupole

Large stresses can break the crust, so one should also ask how large a mountain the star can sustain. This problem has been studied by different authors in Newtonian physics (Ushomirsky et al. 2000; Haskell, Jones & Andersson 2006) and, more recently, in general relativity (Johnson-McDaniel & Owen 2013). The results depend critically on the breaking strain $\bar{\sigma}_{\rm c}$ of the crust, i.e. the average strain $\bar{\sigma} = \bar{T}/\mu$ that can be built up before the crust cracks, where μ is the shear modulus of the crust and $\bar{T}$ the average stress. The breaking strain of a NS crust is not well known, but is known to be $\bar{\sigma}_{\rm c} \approx 10^{-2}$ for perfect crystals in a laboratory setting, and recent molecular dynamics simulations have shown that it may reach $\bar{\sigma}_{\rm c} \approx 10^{-1}$ in NS crusts (Horowitz & Kadau 2009). The maximum quadrupoles that can be sustained are thus of the order of $Q_{22} \approx 10^{38}$–10^{39} g cm^2 for more massive stars ($M \approx 2\,\mathrm{M_\odot}$) and $Q_{22} \approx 10^{39}$–10^{40} g cm^2 for less massive stars ($M \approx 1.2\,\mathrm{M_\odot}$), depending on the exact equation of state.

2.3 Gravitational radiation

It is natural to ask, for the currently known LMXBs, how large a thermal mountain can grow and if it is detectable by current and next generation interferometers, such as ALIGO or the Einstein Telescope (ET). To answer these questions let us examine the LMXBs whose spins are known. They can be divided in two classes: the accreting millisecond X-ray pulsars (AMXPs), which are detected as pulsars and can thus be timed, and the nuclear-powered (NP) pulsars which do not pulsate, but exhibit quasi-periodic oscillations in the tails of type II nuclear bursts. The frequency of these oscillations is a measure of the spin period, as confirmed by observations of burst oscillations in sources that are also detected as X-ray pulsars (Patruno & Watts 2012). The details of the LMXBs we use are presented in Table 1. The other quantities listed in Table 1 are the distance to the source and additionally the average duration Δt and average mass accretion rate $\langle \dot{M} \rangle$ during outbursts. The amount of mass that is accreted during an outburst can then be obtained as $\Delta M = \langle \dot{M} \rangle \Delta t$, and inserted into equation (3) to calculate the temperature increase due to nuclear reactions in the crust.

To calculate the average mass accretion rate for all sources we followed two different approaches. For AMXPs we used the data collected by the *Rossi X-ray Timing Explorer* (*RXTE*) and recorded

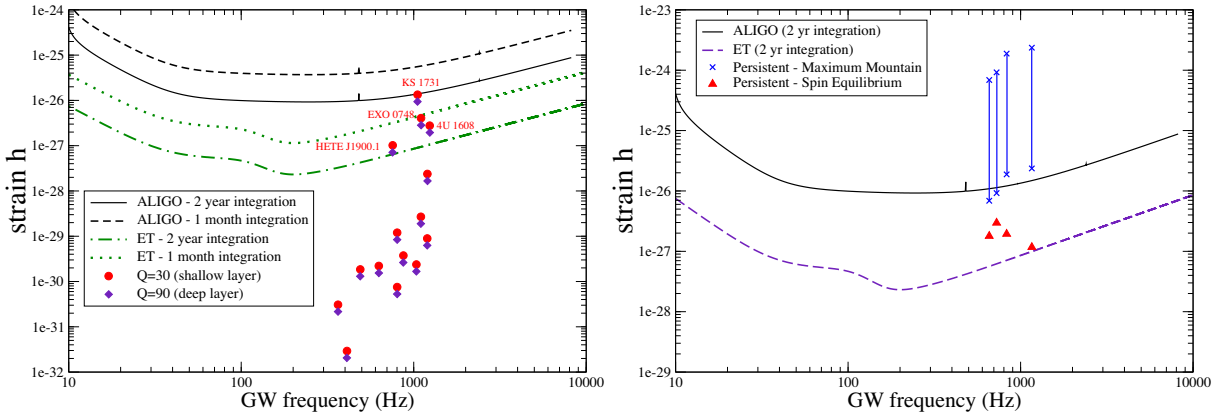

Figure 1. GW strain versus frequency for mountains in AMXPs and NP pulsars. In the left-hand panel we show transient sources, for which the mountain is the largest that can be created during an outburst, both in the case of a shallow ($Q = 30$ MeV) and of a deep ($Q = 90$ MeV) capture layer. In the right-hand panel we show the persistent sources, for which we assume both the maximum mountain the crust can sustain (crosses), and a mountain that would give spin equilibrium from torque balance (solid triangles). The bars indicate the range given by uncertainties on the breaking strain, as described in the text.

with the Proportional Counter Array (PCA; see Jahoda et al. 2006). We used the Standard-2 data mode and extracted the 2–16-keV X-ray fluxes for all outbursts, following the procedure by van Straaten et al. (2003). The fluxes for each outburst were averaged assuming a fiducial spectral index (i.e. assuming that the spectral index remains constant during the course of the outburst and between different outbursts) taken from the literature. We then extrapolated to the 0.1–100 keV (bolometric) flux. We used the unabsorbed luminosity (where we take the hydrogen absorption column $N_{\rm H}$ reported in the literature, see Table 1). The bolometric luminosity was then calculated from the distance in Table 1 and the mass accretion rate as given by $L_{\rm acc} = G\,M\,\dot{M}\,R = \dot{M}\eta\,c^2$. Here, $L_{\rm acc}$ is the bolometric accretion luminosity, and we assumed a mass of $M = 1.4\,{\rm M}_{\odot}$, and a radius $R = 10$ km and η is the conversion efficiency for the rest-mass into energy. After calculating the average mass accretion rate for each outburst we selected (and reported in Table 1) the highest value obtained (i.e. we consider the biggest possible mountain).

For the NP accreting pulsars we used instead data from the All-Sky Monitor (ASM) onboard *RXTE*, which operated in the 1.3–12.1 keV band. We used the ASM rather than the PCA because all the eight sources selected are either persistent sources or have long outbursts. The ASM, being a monitoring instrument, has a much better data coverage (although with lower sensitivity and a narrower energy band). In this case we selected the absorption column $N_{\rm H}$ and spectral index Γ from the literature (whenever available) or, when no spectral analysis was available, used the Galactic $N_{\rm H}$ and a simple power-law model with spectral index $\Gamma = 2$.

We caution that the results may suffer from systematic errors in both distance d and spectral index Γ. However the estimates are likely to be sufficiently accurate for our purposes. The main conclusions of this paper will not change unless there is a substantial error in our assumptions that can change the mass accretion rate by orders of magnitude (e.g. a substantial error in the distance).

2.4 Transient sources

In the left-hand panel of Fig. 1 we show the GW strain corresponding to the maximum mountain that could be created during an outburst (equations 2 and 1), assuming that $\delta T_{\rm q}/\delta T = 0.1$. We consider this to be a reasonable upper limit, as a significantly larger fraction $\delta T_{\rm q}/\delta T$ would lead to detectable pulsations in quiescence for some of the sources, as we shall see in Section 2.6. Note, however, that there is currently no physically motivated estimate for $\delta T_{\rm q}/\delta T$, and the true value may be much smaller. We consider two capture layers, a shallow one close to neutron drip (where most of the heat is predicted to be deposited Haensel & Zdunik 1990) with a threshold of $Q = 30$ MeV, and a deeper layer at a pressure of $p = 10^{32}$ dyn cm^{-2}, with a threshold energy of $Q = 90$ MeV. All values lie below the maximum quadrupole that the crust can sustain. Note also that the increase in the quadrupole Q_{22} due to the higher threshold energy Q is more than offset by the decrease in heating at higher pressures, as obtained from equation (3). The results for the deep and shallow capture layers are thus very similar. The thermal timescale for the deeper capture layers is, however, $\tau_{\rm th} \approx 6$ yr. Hence a 'deep' mountain may never relax entirely in systems such as Aql X-1 that have frequent outbursts, with recurrence times shorter than $\tau_{\rm th}$. These systems may effectively behave as persistent sources for our purposes, and harbour larger mountains.

In the left-hand panel of Fig. 1 we compare our results to the sensitivity achieved by ALIGO (assuming both detectors have the same sensitivity) and ET, first by assuming an integration time of 1 month (an average duration for an outburst) and then of 2 yr. It is quite clear from the figure that, even for a 2 yr integration, most systems fall well below the sensitivity curve. Strain sensitivity curves for ALIGO and ET are, respectively, taken from the public LIGO document[1] and Hild, Chelkowski & Freise (2008). A fully coherent search over time, $T_{\rm obs}$, is sensitive to a strain of

$$h \approx 11.4\sqrt{S_{\rm n}(\nu)/T_{\rm obs}}, \tag{5}$$

where $S_{\rm n}(\nu)$ is the detector noise power spectral density, and the factor 11.4 accounts for a single trial false alarm rate of 1 per cent and a false dismissal rate of 10 per cent (Abbott et al. 2007a; Watts et al. 2008).

It is unlikely that transient systems will be strong enough sources for ALIGO, but they are promising sources for ET. This is essentially the same conclusion of Watts et al. (2008), who considered emission at the torque balance level, which is higher than the strain we calculate (note that both our estimates and those of Watts et al. 2008 assume mountains that are smaller than the maximum that the crust can sustain before breaking). A few systems appear to be close to the threshold for detection. However these systems are

[1] https://dcc.ligo.org/LIGO-T0900288/public

unlikely to be good targets for upcoming GW searches, as they have all just entered quiescence after long outbursts, during which large amounts of mass were accreted and the crust was heated considerably. The mountain is currently relaxing on a time-scale $\tau_{\rm th}$ and the recurrence time between accretion outbursts is likely to be long. It is thus probable that they will not be 'on' as continuous GW sources during ALIGO observations.

2.5 Persistent sources

For the persistently accreting sources the situation is different. We assume that ongoing accretion builds the largest mountain that can be sustained. We take the quadrupole to be in the range $10^{38}\,{\rm gcm}^2 \lesssim Q_{22} \lesssim 10^{40}\,{\rm gcm}^2$, to account for the uncertainty in mass and equation of state, as estimated by Johnson-McDaniel & Owen (2013). The results are shown in the right-hand panel of Fig. 1. The error bars account for the range discussed above. We also present the torque balance upper limits on Q_{22}, as in Watts et al. (2008). The results for the maximum mountain comfortably exceed the torque balance limits. If accretion is ongoing, the quadrupole can thus become larger than the value needed for torque balance. In this scenario there is thus a net spin-down torque due to GW emission, and the prediction for the spin-down rate is

$$\dot{\nu} \approx -6 \times 10^{-13} \left(\frac{\nu}{500\,{\rm Hz}}\right)^5 \left(\frac{Q_{22}}{10^{38}\,{\rm g\,cm}^2}\right) \,{\rm Hz\,s}^{-1} \qquad (6)$$

(where we have assumed a moment of inertia $I = 10^{45}$ g cm^2 for the star). Such spin-down is sufficiently strong to be detectable with current instrumentation. However, none of the persistent sources considered here have ever shown accretion powered pulsations that would allow us to test this prediction. Continued deep searches for pulsations from these objects is thus of significant importance for GW science.

Another issue to consider is the amount of internal heating required to sustain a large quadrupole. Rearranging equation (3) we see that, for a fiducial star of radius $R = 12$ km, one has

$$\delta T_{\rm q} \approx 3 \times 10^7 \left(\frac{Q_{22}}{10^{38}\,{\rm g\,cm}^2}\right) \left(\frac{30\,{\rm MeV}}{Q}\right)^3 \,{\rm K}. \qquad (7)$$

For hot sources with internal temperatures $T = 10^8$ K, high values of the quadrupole (around $Q_{22} \approx 10^{39}$ g cm^2) would require $\delta T_{\rm q}/T > 1$, even for deeper capture layers. Such high values of $\delta T_{\rm q}/T > 1$ would lead to pulsations in quiescence at a level that is not observed. However for lower values of Q_{22}, deeper capture layers and higher activation energy Q, the temperature perturbation is $\delta T_{\rm q}/T \leq 0.1$. During accretion outbursts the resulting perturbations to the luminosity are $\delta L_{\rm bol} \lesssim 10^{32}\,{\rm erg\,s}^{-1}$, and are not visible (Ushomirsky et al. 2000), as the emission is at much higher levels ($L_{\rm bol} = L_{\rm acc} \simeq 10^{35}$–$10^{37}\,{\rm erg\,s}^{-1}$). However such levels of heating can make the quiescent flux vary, as we argue below.

We can summarize the discussion above by asking what a GW detection implies for deep crustal heating. We use equations (1) and (2) to represent the sensitivity curve of ALIGO and ET in terms of an equivalent quadrupolar temperature deformation $\delta T_{\rm q}$, as shown in Fig. 2. We consider two fiducial systems at a distance $d = 5$ kpc: a system that undergoes shorter outbursts and is colder ($T = 5 \times 10^7$ K), for which we integrate the GW signal over the fiducial duration of the outburst (1 month); and a hotter ($T = 5 \times 10^8$ K), persistent system for which we integrate the GW signal over a 2 yr period. Fig. 2 shows that ALIGO and ET will probe the $\delta T_{\rm q}/T \approx 0.1$ regime, with ET probing the possibly more realistic $\delta T_{\rm q}/T \leq 0.01$ regime. This is also the order of magnitude of the perturbations

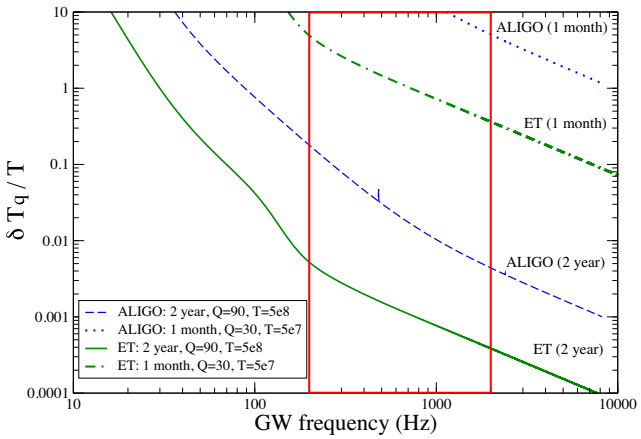

Figure 2. Sensitivity of current and next generation GW detectors to gravitational waves sourced by quadrupolar temperature deformations $\delta T_{\rm q}$ in deep ($Q = 90$ MeV) and shallow ($Q = 30$ MeV) layers of the NS crust. The GW strain is expressed in terms of the temperature perturbations $\delta T_{\rm q}/T$ that give rise to the mountain, as described in the text. Both second and third generation detectors will probe regimes of physical interest, with ALIGO probing the $\delta T_{\rm q}/T \approx 0.1$ regime, and ET the $\delta T_{\rm q}/T \approx 0.01$ regime. We show the sensitivity of ALIGO both for a 1 month integration, $Q = 30$ MeV, and background temperatures $T = 5 \times 10^7$ K (dotted curve), corresponding to the case of a short outburst, and for a 2 yr integration, $Q = 90$ MeV, and a background temperature of $T = 5 \times 10^8$ K (dashed curve), more appropriate for a persistent system. Similarly we show the sensitivity of ET for $T = 5 \times 10^7$ K, $Q = 30$ MeV, and a 1 month integration (dot–dashed curve) and $T = 5 \times 10^8$ K, $Q = 90$ MeV, and a 2 yr integration (solid line curve). The region enclosed by the red box is that most relevant for LMXBs.

expected in the quiescent flux (see Section 2.6), which may be detectable with future X-ray satellites such as the Large Observatory for X-ray Timing (LOFT) or the Neutron star Interior Composition Explorer (NICER).

In the analysis above we make many approximations. First and foremost we only consider two capture layers in the stars. In reality all layers contribute to Q_{22}, leading to larger quadrupoles than those discussed above (Ushomirsky et al. 2000). For shorter outbursts the reduced heating at higher densities offsets the higher quadrupole Q_{22} in those regions. The reactions that deposit the most heat thus dominate, independently of density. We are accounting for what is considered to be the most important layer at neutron drip (Haensel & Zdunik 1990), so unless there is significantly more heating in deeper layers that previous calculations have not accounted for, it is unlikely that our results severely underestimate Q_{22}. In general the result of our analysis is that thermal mountains on NSs in transient LMXBs are likely to be very challenging to detect, even with third generation detectors. Persistent systems, however, offer a promising target and electromagnetic observations may allow further constraints on the physics of the system, as we shall see in Section 3.4.

2.6 X-ray flux variations

We now focus on the observable X-ray flux variations induced by a thermal perturbation due to a mountain in the crust. As already discussed we restrict our attention to perturbations of the thermal quiescent emission. We thus assume that a mountain has been created during an accretion outburst, and study how the associated thermal perturbations evolve as the system returns to quiescence. To understand how the surface flux is affected we consider the quadrupolar flux variations as linear perturbations on a spherically

symmetric background. We start by obtaining the spherical background model for the temperature profile from the Newtonian heat transport equations in the crust:

$$C_v \frac{\partial T}{\partial t} = \nabla(K \nabla T) - \rho\epsilon, \tag{8}$$

where T is the temperature, C_v the heat capacity, K the conductivity, ρ the density and $\epsilon = \epsilon_\nu - \epsilon_h$, with ϵ_ν the neutrino emissivity and ϵ_h the energy deposition rate. To simplify our treatment and make a first assessment of detectability, we will use an $n = 1$ polytrope for the equation of state, and analytic expressions for the contribution of electrons in the crust to the conductivity (Flowers & Itoh 1981) and specific heat (Maxwell 1979), from which one obtains

$$K = 10^{16} \left(\frac{\rho}{10^6\,\mathrm{g\,cm^{-3}}}\right)^{1/3} \left(\frac{T}{10^8\,\mathrm{K}}\right)\ \mathrm{erg\,(cm\,s\,K)^{-1}}, \tag{9}$$

$$C_v = 3.72 \times 10^{17} \left(\frac{\rho}{\rho_0}\right)^{4/3} \left(\frac{T}{10^8\,\mathrm{K}}\right)\ \mathrm{erg\,(cm^3\,K)^{-1}}, \tag{10}$$

where ρ_0 is the nuclear saturation density. We set $\epsilon_h = 0$ (note this is true for the background, but for the perturbations we will have $\delta\epsilon_h \neq 0$), and for the neutrino emissivity we approximate the results of Haensel, Kaminker& Yakovlev (1996) for $\nu\bar{\nu}$ electron Brehmstrahlung as

$$\epsilon_\nu = 6.46 \times 10^{18} \left(\frac{\rho}{10^{12}\,\mathrm{g\,cm^{-3}}}\right) \left(\frac{T}{10^9\mathrm{K}}\right)^6\ \mathrm{cm^2\,s^{-3}}. \tag{11}$$

At the boundary with the core we assume a constant temperature and for the outer boundary we assume that the emission from the surface is thermal, i.e. $-K\nabla T = (R^2/R_*^2)\sigma T_s^4$, with σ the Stefan–Boltzman constant. The stellar radius is R, and R_* is the radius at which we fix the outer boundary of our numerical grid. The surface temperature T_s at R is then obtained from the temperature T at R_* using the prescription of Gudmundsson, Pethick & Epstein (1983):

$$\left(\frac{T_s}{10^6\,\mathrm{K}}\right) = g_{14} \left(18.1 \frac{T}{10^9\,\mathrm{K}}\right)^{2.42}, \tag{12}$$

with g_{14} the gravitational acceleration in units of 10^{14} cm s^{-2}. Note that one can model the composition of the outer layers in more detail (see e.g. Haskell et al. 2012; Mahmoodifar & Strohmayer 2013). However, given the many simplifying assumptions and the uncertainties associated with the measurements in Table 1, we use the expression in equation (12), as it is unlikely to be the main source of error in our analysis.

We obtain our background model by specifying a core temperature at the inner boundary (the crust/core interface) and evolving equation (8) until we obtain an equilibrium. We are now ready to evolve the quadrupolar temperature perturbations due to the mountain on this background. The evolution equation for an $l = m = 2$ perturbation takes the form (Ushomirsky et al. 2000)

$$C_v \frac{\partial \delta T_q}{\partial t} = -\frac{1}{r^2}\frac{\partial}{\partial r}\left(r^2 K \frac{\partial \delta T_q}{\partial r}\right) - l(l+1)\frac{K \delta T_q}{r^2} + \rho\epsilon\left(\frac{\delta K}{K} - \frac{\delta\epsilon}{\epsilon}\right) + F_Q \frac{\partial}{\partial r}\left(\frac{\delta K}{K}\right), \tag{13}$$

with $F_Q = -K\nabla T$ the background flux obtained from the equilibrium solution of equation (8). We obtain δK from equation (9) with the condition $\delta\rho = 0$, as in Ushomirsky et al. (2000). At the boundary with the core we assume that $\delta T_q = 0$, while at the outer boundary we perturb the thermal flux condition, so that one has $\delta F = 4(R^2/r^2)\sigma T_s^3 \delta T_q^s$, with

$$\left(\frac{\delta T_q^s}{10^6\,\mathrm{K}}\right) = 2.42\, g_{14} \left(18.1 \frac{T}{10^9\,\mathrm{K}}\right)^{2.42} \frac{\delta T_q}{T}. \tag{14}$$

We take $\delta\epsilon = \delta\epsilon_h$ and assume $\delta\epsilon_h$ to be due to quadrupolar energy deposition in the capture layers. For the deep capture layer, we specify an energy deposition term $\delta\epsilon_h$ with a Gaussian radial profile, located at a pressure of $P = 10^{32}$ dyn cm^{-2}, and with a half-width of 5 m for the deep capture layer, and at $P = 10^{30}$ dyn cm^{-2} and with a half-width of 1 m for the shallow layer. Evolving equation (13) we find that, as the problem is linear in the perturbations, to a very good approximation the following relations hold:

$$\frac{\delta F}{F_Q} \approx 1.29 \frac{\delta T_q}{T}, \quad \text{(deep layer)} \tag{15}$$

$$\frac{\delta F}{F_Q} \approx 1.48 \frac{\delta T_q}{T}, \quad \text{(shallow layer)} \tag{16}$$

with very little dependence on the chosen background temperature T. We remind the reader that we are normalizing to the quiescent (thermal) flux F_Q obtained from the equilibrium solution of equation (8).

In quiescence the quadrupolar temperature perturbations associated with a mountain and GW emission (equations 2 and 3) thus perturb the X-ray flux from the surface (equations 15 and 16), and as the star rotates this leads to pulsations at twice the rotation frequency (i.e. the same frequency as the GWs). In Fig. 3 we show the sensitivity curve for ALIGO and ET in terms of an equivalent pulsed fraction of the X-ray flux. We can see that if it is possible to integrate the signal for 2 yr (physically this corresponds to a capture layer deep enough that $\tau_{\rm th} \gg 2$ yr, and the mountain is not dissipated significantly during the observation), both ALIGO and ET can probe an interesting region of parameter space, with $\delta F/F_Q \lesssim 0.01$.

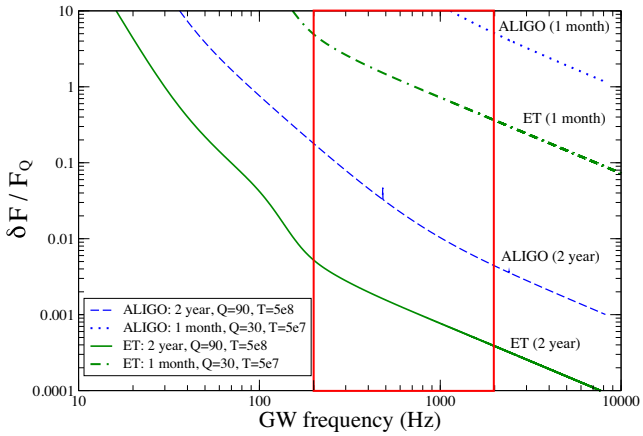

Figure 3. The pulsed fraction $\delta F/F_Q$ corresponding to a GW detection at threshold (as obtained from equation 5) for ALIGO and ET. For deep capture layers ($Q = 90$ MeV) and a background temperature of $T = 5 \times 10^8$ K, we show the results for an integration time of 2 yr (dashed curve for ALIGO, solid curve for ET). Physically this is due to the fact that in the deep crust $\tau_{\rm th} > 2$ yr, and the mountain will thus not relax significantly during the observation. For shallow capture layers ($Q = 30$ MeV) and $T = 5 \times 10^7$ K, we show the results for an integration time of 1 month (dotted curve for ALIGO, dot–dashed curve for ET). The region enclosed by the red box is the region of interest for LMXBs.

3 MAGNETIC MOUNTAINS

3.1 Hydromagnetic evolution

Accretion not only perturbs the structure of the star by affecting nuclear reactions in the crust, but it also deforms the stellar magnetic field. As matter is accreted and spreads towards the equator it drags the field with it, and compresses it. This leads to a *locally* strong field that can sustain a 'magnetic' mountain (Payne & Melatos 2004; Melatos & Payne 2005; Vigelius & Melatos 2009b). This can lead to much larger deformations than those due to the overall background magnetic field, even if the internal toroidal component of the field is much stronger than the inferred external magnetic dipole (Ciolfi & Rezzolla 2013). Recent calculations have shown that for realistic equations of state the mountain could lead to a detectable GW signal (Priymak et al. 2011). Note also that magnetic mountains are not sustained by crustal rigidity and the resulting quadrupole can thus be larger than the value required to crack the crust.

One of the main differences with respect to thermal mountains is that the time-scale on which a magnetic deformation relaxes, after an outburst, is not the thermal time-scale $\tau_{\rm th}$, but the slower Ohmic dissipation time-scale $\tau_{\rm o} \geq 10^8$ yr (Vigelius & Melatos 2009b). Hence a mountain forms gradually over several outbursts. Grad–Shafranov calculations indicate that the hydromagnetic structure of a mountain conforms to a single-parameter family of solutions which, once the size of the accreting polar cap is fixed, are function only of the mass accreted over the systems lifetime, $M_{\rm a}$. This suggests that magnetic mountains can be treated as the persistent sources of the previous section. The main difference is that the quadrupole does not depend on crustal rigidity, but on the magnetic field strength when accretion begins, which we denote B_* (note that this is different from, and generally lower than, the expected NS magnetic field at birth, as obtained from population synthesis models Faucher-Giguère & Kaspi 2006), the initial field structure and $M_{\rm a}$ (Payne & Melatos 2004; Melatos & Payne 2005; Priymak et al. 2011).

As more mass is accreted the external dipolar component of the field, $B_{\rm ext}$, is quenched according to Shibazaki et al. (1989):

$$B_{\rm ext} = B_* \left(1 + \frac{M_{\rm a}}{M_{\rm c}}\right)^{-1}, \tag{17}$$

and the mass quadrupole is given by

$$Q_{22} \approx 10^{45}\, A \left(\frac{M_{\rm a}}{\rm M_\odot}\right) \left(1 + \frac{M_{\rm a}}{M_{\rm c}}\right)^{-1} \ {\rm g\ cm^2}, \tag{18}$$

where $A \approx 1$ is a geometric factor that depends on the equation of state and accretion geometry (Melatos & Payne 2005), while $M_{\rm c}$ is the critical amount of accreted matter at which the mechanism saturates, which also depends on the equation of state (Priymak et al. 2011). The estimates above are valid to leading order in $M_{\rm a}/M_{\rm c}$; for $M_{\rm a} \approx M_{\rm c}$ they are no longer accurate and numerical solutions are necessary. General relations for the critical mass were derived by Melatos & Payne (2005) and Payne & Melatos (2004) for isothermal mountains, while for more realistic equations of state (models C and E of Priymak et al. 2011), one has $M_{\rm c} \approx 10^{-7} (B_*/10^{12}\ {\rm G})^{4/3}\ {\rm M_\odot}$. In the regime $M_{\rm a} \gg M_{\rm c}$, both relations are expected to deviate significantly from the simple estimates above in equations (17) and (18). Numerical simulations cannot probe this regime; instead one finds that, for $M_{\rm a} \gtrsim M_{\rm c}$ one has $0.01 \leq B_{\rm ext}/B_* \leq 0.1$ and quadrupoles in the range $10^{37} \lesssim Q_{22} \lesssim 10^{38}$ g cm^2, for an initial field of $B_* = 10^{12.5}$ G. Note, however, that the main difficulty in pushing the simulations to $M_{\rm a} > 10 M_{\rm c}$ is numerical. The only firm upper limit on the suppression of the external dipole field come from Ohmic diffusion, which limits the burial of the field at a level of $B_{\rm ext}/B_* \approx 10^{-4}$ (Vigelius & Melatos 2009b).

3.2 Pre-accretion magnetic field

What limits can we set on B_*, the strength of the magnetic field at the onset of accretion? Observational constraints can be obtained from measurements of the spin-down between outbursts for four systems (see Patruno & Watts 2012 and references therein), which are consistent with $B_{\rm ext} \approx 10^8$ G. The magnetic fields inferred for millisecond radio pulsars are also in the range $B_{\rm ext} \approx 10^8$ G. Furthermore observations of a slow (11 Hz) pulsar in Terzan 5, IGR J17480−2446, indicate that this system, which is thought to have been accreting for a shorter period of time than most of the LMXB population, may have a stronger field $10^9\ {\rm G} \lesssim B_{\rm ext} \lesssim 10^{10}$ G (Cavecchi et al. 2011). It is thus plausible that one starts with $B_* \gtrsim 10^9$ G, and that the external field is reduced to $B_{\rm ext} \approx 10^8$ by accretion.

If $B_* \gtrsim 10^{11}$ G, and polar magnetic burial is very short lived, we would expect $B_{\rm ext} \approx B_*$ in the millisecond radio pulsars (unless accretion leads to significant dissipation of the field; Konar & Bhattacharya 1997, 1999). This would lead to larger spin-down rates than those observed. On the other hand, if the field remains buried and the magnetic mountain is stable on long time-scales (as simulations by Vigelius & Melatos 2009b indicate), then the results of Priymak et al. (2011) imply a quadrupole $Q_{22} > 10^{36} (B_*/10^{11}\ {\rm G})^{4/3}$ g cm^2 for $M_{\rm a} = M_{\rm c}$. From equation (6), this gives a spin-down rate $\dot{\nu} > 10^{-14}$ Hz s^{-1} for a 500 Hz pulsar, close to the maximum spin-down rates measured for millisecond pulsars. High initial fields of $B_* \gtrsim 10^{11}$ G would thus challenge current observations.

3.3 Gravitational radiation

In the left-hand panel of Fig. 4 we plot GW strain versus frequency for magnetic mountains that do not decay between outbursts. We consider first a scenario in which $B_* \approx 10^{10}$ G and the critical mass $M_{\rm c}$ has been accreted over a system's lifetime (i.e. $M_{\rm a} = M_{\rm c}$). The GW emission is predictably weak. Given the uncertainties associated with modelling field burial, in Fig. 4 we also consider the case in which the birth field is $B_* \approx 10^{12}$ G. In this case some of the systems could be emitting detectable gravitational radiation, and a detection would provide evidence for a high degree of field burial. The latter scenario can be excluded in the three systems (SAX J1808.4−3658, XTE J1751−305, IGR J00291+5934; Patruno & Watts 2012) for which we have a measured spin-down between outbursts. In all cases the spin-down rate is $\dot{\nu} \approx -10^{-15}$ Hz s^{-1} and it implies an upper limit of $Q_{22} \approx 10^{36}$ g cm^2, if we assume that GW emission is the dominant spin-down mechanism. GW emission at this level, due to a magnetic mountain, implies $B_* \approx 5 \times 10^{10}$ G and would be unlikely to be detected, as can be seen from Fig. 4. For our models with $M_{\rm a} = M_{\rm c}$, $B_* \approx 5 \times 10^{10}$ G leads to $B_{\rm ext} \approx 2.5 \times 10^{10}$ G (Priymak et al. 2011). Such a strong dipole field would, however, lead to a greater than observed spin-down due to magnetic dipole radiation. In fact, if the spin-down is attributed to dipole radiation, the implied magnetic field is $B_{\rm ext} \approx 10^8$ G for all these systems (Patruno & Watts 2012). An upper limit of $|\dot{\nu}| < 2 \times 10^{-15}$ Hz s^{-1} also exists on the spin-down rate of Swift J1756.9−2508. In this case the limit on the dipole field from electromagnetic spin-down is of $B_{\rm ext} \lesssim 5 \times 10^8$ G but the field needed to explain the spin-down in terms of GWs from magnetic mountains is $B_* \approx 10^{12}$ G corresponding to $B_{\rm ext} \approx 5 \times 10^{11}$ G for $M_{\rm a} = M_{\rm c}$ in our models. It is important

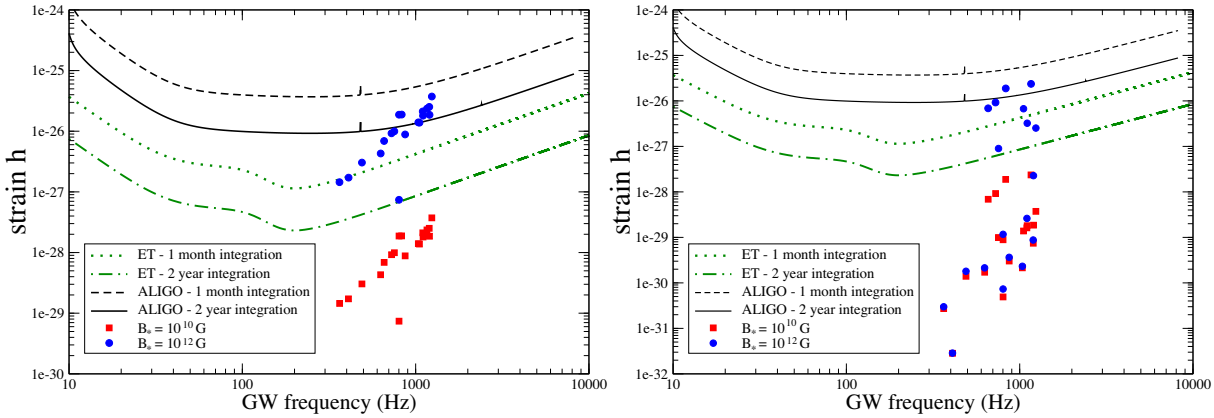

Figure 4. GW strain versus frequency for the systems in Table 1, for two magnetic mountain scenarios. In the left-hand panel we show the strain that can be achieved assuming that the magnetic mountain does not decay between accretion outbursts, for two values of the magnetic field at the onset of accretion, $B_* = 10^{10}$ and 10^{12} G. In the right-hand panel we consider the scenario in which the mountain decays between outbursts. Detection will be very challenging for both ALIGO and ET, unless $B_* \approx 10^{12}$ G.

to note though that while simulations indicate that the quadrupole saturates for $M_a \gtrsim M_c$ (Wette, Vigelius & Melatos 2010), no such effect is observed for the decay of the external field, and the limits on evolving the field further are mainly numerical. One cannot thus exclude high degrees of field burial. In fact the harmonic content of thermonuclear bursts suggests that in some systems burning occurs in patches and is confined by locally strong and compressed magnetic fields (Bhattacharyya & Strohmayer 2006; Misanovic, Galloway & Cooper 2010; Cavecchi et al. 2011; Chakraborty & Bhattacharyya 2012).

We also analyse the scenario in which the magnetic mountain decays on short time-scales between accretion outbursts. Time-dependent MHD simulations show that magnetic line tying at the stellar surface stabilizes the mountain against interchange instabilities. Current-driven Parker-type instabilities do occur, but they do not disrupt the mountain, saturating in a state where the quadrupole is reduced by $\lesssim 60$ per cent (Vigelius & Melatos 2009b). Simulations confirm stability up to the tearing-mode time-scales but they do not resolve slower instabilities and modes below the grid scale. Different choices of boundary conditions can also destabilize the system (Mukherjee, Bhattacharya & Mignone 2013a,b). In this scenario we take $M_a = \Delta t \langle \dot{M} \rangle$ for each system, and calculate the quadrupole from equation (18). The results for the predicted GW strain are shown in the right-hand panel of Fig. 4. This scenario leads to small mountains and weak GW emission, that would be undetectable for most systems, even for ET. The only systems that would lead to detectable GWs are the persistent ones, if $B_* \approx 10^{12}$ G.

In Fig. 5 we show the GW strain expressed in terms of an equivalent B_{ext} obtained from equation (18), using model E of Priymak et al. (2011) and $M_a = M_c$, for which $B_{ext} = B_*/2$. We can see that ALIGO is expected to probe high field scenarios, with 10^{11} G $\lesssim B_* \lesssim 10^{12}$ G, while ET will probe a physically more realistic section of parameter space, i.e. $B_* < 10^{11}$ G.

3.4 Distinguishing magnetic from thermal mountains

An interesting question is if, given a GW detection, it would be possible to understand whether we are observing a thermal or magnetic mountain. We have already discussed the electromagnetic counterpart of a thermal mountain in Section 2.6, and showed that a quadrupolar deformation could lead to flux modulations and pulsations in quiescence at twice the spin frequency. The results of

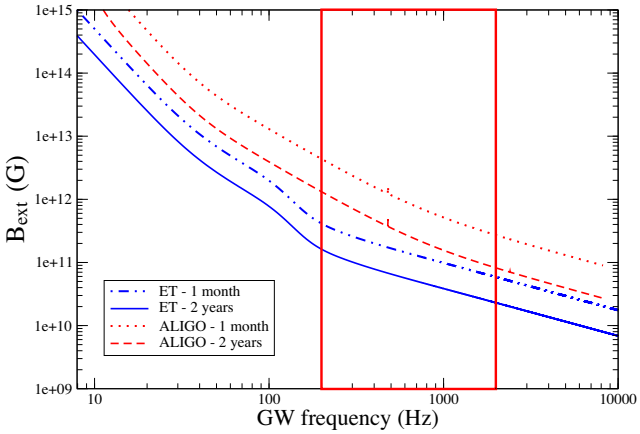

Figure 5. The sensitivity of ALIGO and ET to a magnetic mountain. The GW strain is expressed in terms of the magnetic field B_{ext} of the star, for a fiducial system at 5 kpc and model E of Priymak et al. (2011). We take $M_a = M_c$ and, as described in the text, one has $B_{ext} = B_*/2$ for these models. We plot both the case of a 1 month integration (dot–dashed curve for ET and dotted curve for ALIGO) and a 2 yr integration (solid curve for ET and dashed curve for ALIGO). We can see ALIGO will probe high field scenarios, with 10^{11} G $\lesssim B_{ext} \lesssim 10^{12}$ G, while ET will be able to probe fields of $B_{ext} < 10^{11}$ G.

the previous section suggest that if a magnetic mountain were to be detected in a hypothetical system, such an NS would have a strong 'birth' (i.e. at the onset of the LMXB phase) magnetic field $B_* \approx 10^{12}$ G, although the external dipolar field may be lower, due to accretion induced magnetic burial. In such a circumstance cyclotron resonance scattering features should appear in the X-ray emission and Priymak, Melatos & Lasky (2014) have studied the problem in detail for the case of an accretion buried field. We repeat the analysis here for a 1.4 $M_\odot$ NS with an accreted outer envelope described by the equation of state E of Priymak et al. (2014). We vary B_* between 10^{11} and 10^{12} G and study the emission features for $M_a = M_c$. In Fig. 6 we show an example of the kind of spectra that such a set-up produces. The solid line represents the phase-averaged spectrum, while the dotted lines represent phase-resolved spectra for two extreme rotational phases, $\omega = \pi/2$ and $\omega = 3\pi/2$. We can see that in all cases the energy of the first line is fairly stable, but the depth can vary strongly with phase, as can the shape of the higher

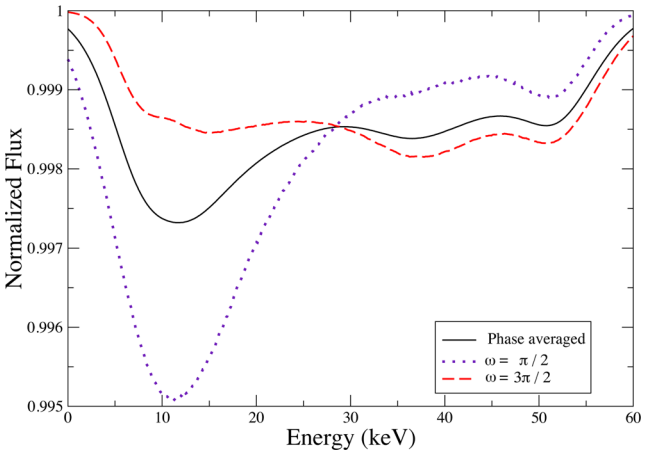

Figure 6. Example of a cyclotron spectrum, obtained with the code of Priymak et al. (2014) for a $M = 1.4\,\mathrm{M}_\odot$ NS described by equation of state E, with the following parameters: $\iota = \pi/4$ (observer inclination relative to the rotation axis), $\alpha = \pi/4$ (inclination of the magnetic axis relative to the rotation axis), $B_* = 10^{12.8}$ G, $M_\mathrm{a} = M_\mathrm{c} = 3.014\,26 \times 10^{-7}\,\mathrm{M}_\odot$ (see Priymak et al. 2014 for a full description of the parameters). The solid line represents the phase-averaged spectrum, while the dashed and dotted lines represent the phase-resolved spectra for two extreme rotational phases, $\omega = \pi/2$ (dashed line) and $\omega = 3\pi/2$ (dotted line). While the energy of the lines remains fairly constant the depth varies significantly with phase. The flux is normalized to give unit peak flux.

energy features. A strong phase dependence of the fundamental line for different sizes of polar mountains has also been found by Mukherjee, Bhattacharya & Mignone (2012).

Let us focus on the phase-averaged spectrum. Our simulations show that for $B_* \lesssim 10^{12}$ G no cyclotron resonance scattering features are present. The results for higher field strengths are shown in Fig. 7, where we plot the difference in depth between the first and second line and the ratio between the energies at which the lines appear, versus the pre-accretion magnetic field B_*. The effects are small, but may be measurable by future X-ray observatories such as NICER and LOFT, which will both be capable of resolving modulations of less than 1 per cent at energies of $\approx$1 keV (Feroci et al. 2012; Gendreau, Arzoumanian & Okajima 2012). Furthermore the cyclotron features appear to be more pronounced in the region of interest, i.e. the field strengths that would lead to GW emission at the ALIGO and ET threshold. This method thus has the potential to be a good diagnostic for distinguishing different kinds of continuous GW emission. Additionally instruments such as NICER and LOFT will also be able to carry out phase-resolved spectroscopy, allowing for a much more detailed characterization of the cyclotron resonance scattering features in these systems, which can vary significantly with phase, as illustrated in Fig. 6.

We stress here that no cyclotron lines have been detected in LMXBs containing NSs rotating with millisecond periods, and the fields of these systems are generally thought to be reasonably weak ($B_\mathrm{ext} \approx 10^8$ G). Nevertheless if an as yet unobserved system (e.g. a system that is currently in quiescence) were to become visible and emit detectable GWs, the presence of a cyclotron line would point to a magnetic mountain. Its absence, on the other hand, combined with the estimates in Section 5, would suggest that the quadrupole is more likely to be due to thermally generated crustal mountain (although mountains in the core of the star are also a possibility; Haskell et al. 2007). Especially for weaker fields, however, several combinations of orientation and inclination could lead to cyclotron resonance scattering features not being detectable (see Priymak et al. 2014 for an in depth discussion), so their absence is inconclusive.

4 CONCLUSIONS

In this paper we assess the likely GW signal strength and detection prospects for deformations, or 'mountains' on NSs in LMXBs. Unlike most previous work on this topic we do not assume that the GW spin-down torque has to balance the accretion induced spin-up torque, as several studies have indicated that this is unlikely to be the case for many systems (Andersson et al. 2005; Haskell & Patruno 2011; Patruno et al. 2012). Rather, we calculate the GW signal strength due to the two main mechanisms that have been suggested for building a mountain: asymmetric thermal deposition in the crust (thermal mountains) and magnetically confined mountains (magnetic mountains). We calculate the GW strain for both mechanisms in known LMXBs for which we can measure the spin frequency, average accretion rate during outbursts and outburst duration.

One of the main uncertainties is the time-scale on which the mountain is stable once accretion ceases and the system enters

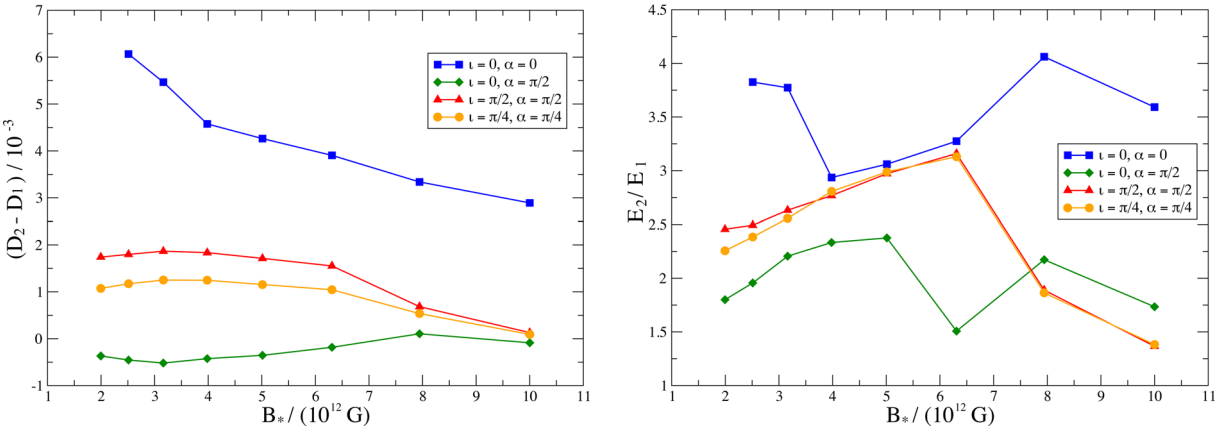

Figure 7. Difference in depth D in normalized flux units (left-hand panel) and ratio between the energies (right-hand panel) of the second and first cyclotron line for a $1.4\,\mathrm{M}_\odot$ NS obtained with model E of Priymak et al. (2014), for varying field strengths B_*. The different colours represent different inclinations of the observer (ι) and of the magnetic field axis (α) with respect to the rotational axis: $\iota = 0, \alpha = 0$ (squares), $\iota = 0, \alpha = 0.5\pi$ (diamonds), $\iota = 0.5\pi, \alpha = 0.5\pi$ (triangles), and $\iota = 0.25\pi, \alpha = 0.25\pi$ (circles). For $B_* < 10^{12}$ the features cannot be distinguished.

quiescence. For thermal mountains it is likely that the quadrupole will dissipate on a thermal time-scale $\tau_{\rm th} \lesssim 6$ yr, leading to large mountains only in persistently accreting systems. In this scenario the GW signal strength for most transient systems falls below the level that would be detectable by ALIGO or ET. In the case of persistent systems, however, the mountain could be even larger than what is required for torque balance, if the crust is as strong as predicted by simulations (Horowitz & Kadau 2009). This would not only lead to detectable GWs, but also predicts a spin-down rate of the NS that could be measurable if accretion powered pulsations were to be discovered from these systems. Continued deep searches for pulsations from luminous LMXBs, such as Sco X-1, are thus complimentary to ongoing GW searches from these systems (Aasi et al. 2014b) and could provide crucial constraints.

For the magnetic case simulations indicate that the mountain could be stable on long time-scales (essentially the Ohmic dissipation time-scale $\tau_{\rm o} \approx 10^8$ yr), building up over multiple accretion outbursts. The size of the mountain is strongly dependent on the strength of the magnetic field when accretion begins, B_*. This is not well constrained, but the systems we consider are old systems, in which the magnetic field is thought to have decayed and to be weak. For both LMXBs and millisecond radio pulsars (that are expected to form mostly from LMXBs) the inferred *exterior* field strengths are $B_{\rm ext} \approx 10^8$ G. The exterior dipolar field will, however, be quenched as the magnetic field is buried by accretion. Our simulations suggest that the exterior field will be reduced by approximately two orders of magnitude (Payne & Melatos 2004; Priymak et al. 2011), but the process does not appear to saturate, and the limits on pushing the results further are mainly numerical. Further field burial is thus possible. We consider two scenarios: one in which $B_* = 10^{10}$ G and the other in which $B_* = 10^{12}$ G. For $B_* \approx 10^{10}$G the detection prospects for magnetic mountains are pessimistic. For a detection with ALIGO or ET it is necessary to have an initial magnetic field $B_* \approx 10^{12}$ G. Although this appears unlikely for currently observed LMXB systems, for which the evidence suggests weakly magnetized NSs (D'Angelo et al. 2014), the process of magnetic burial is still not well understood, and such high values of the background field cannot be excluded.

Finally, it is interesting to note that if a mountain is detected by LIGO or ET, it could be possible to distinguish between a thermal and a magnetic mountain. For the relatively high values of the magnetic field $B_* \approx 10^{12}$ G that make the magnetic mountain detectable one would, in fact, expect phase-dependent and non-trivial cyclotron resonance scattering features to be present in the X-ray spectrum. We calculate examples of such features and show that they could be detected by future X-ray observatories, such as LOFT or NICER. A detection of a GW signal combined with a detection of cyclotron features would provide a strong direct indication of a magnetic mountain and of a large buried magnetic field.

ACKNOWLEDGEMENTS

BH acknowledges the support of the Australian Research Council (ARC) via a Discovery Early Career Researcher Award (DECRA) fellowship. This work is also supported by an ARC Discovery Project grant.

REFERENCES

Aasi et al., 2014a, Phys. Rev. D, 90, 062010
Aasi et al., 2014b, Phys. Rev. D, 91, 062008
Abadie et al., 2011, Phys. Rev. Lett., 107, 271102
Abbott et al., 2007a, Phys. Rev. D, 76, 082001
Abbott et al., 2007b, Phys. Rev. D, 76, 082003
Alpar M. A., Cheng A. F., Ruderman M. A., Shaham J., 1982, Nature, 300, 728
Andersson N., 1998, ApJ, 502, 708
Andersson N., Kokkotas K. D., Stergioulas N., 1999, ApJ, 516, 307
Andersson N., Glampedakis K., Haskell B., Watts A. L., 2005, MNRAS, 361, 1153
Bhattacharyya S., Strohmayer T. E., 2006, ApJ, 641, L53
Bildsten L., 1998, ApJ, 501, L89
Brown E. F., Bildsten L., Rutledge R. E., 1998, ApJ, 504, L95
Cavecchi Y. et al., 2011, ApJ, 740, L8
Chakrabarty D., Morgan E. H., Muno M. P., Galloway D. K., Wijnands R., van der Klis M., Markwardt C. B., 2003, Nature, 424, 42
Chakraborty M., Bhattacharyya S., 2012, MNRAS, 422, 2351
Ciolfi R., Rezzolla L., 2013, MNRAS, 435, L43
Cook G. B., Shapiro S. L., Teukolsky S. A., 1994, ApJ, 423, L117
Cutler C., 2002, Phys. Rev. D, 66, 084025
D'Angelo C. R., Fridriksson J. K., Messenger C., Patruno A., 2014, MNRAS, 449, 2803
Degenaar N. et al., 2011, MNRAS, 412, 1409
Degenaar N. et al., 2013, ApJ, 775, 48
Egron E. et al., 2011, A&A, 530, 99
Falanga M. et al., 2005, A&A, 444, 15
Falanga M. et al., 2011, A&A, 529, 68
Falanga M., Kuiper L., Poutanen J., Galloway D. K., Bozzo E., Goldwurm A., Hermsen W., Stella L., 2012, A&A, 545, 26
Faucher-Giguère C.-A., Kaspi V., 2006, ApJ, 643, 332
Feroci M. et al., 2012, Exp. Astron., 34, 415
Ferrigno C. et al., 2011, A&A, 525, 48
Ferrigno C. et al., 2014, A&A, 567, A77
Flowers E., Itoh N., 1981, ApJ, 250, 750
Gendreau K. C., Arzoumanian Z., Okajima T., 2012, in Takahashi T., Murray S. S., den Herder J.-W. A., eds, Proc. SPIE Conf. Ser. Vol. 8443, Space Telescopes and Instrumentation 2012: Ultraviolet to Gamma Ray. SPIE, Bellingham, p. 844313
Gierlinski M., Done C., 2002, MNRAS, 337, 1373
Goetz E., Riles K., 2011, Class. Quantum Gravity, 28, 215006
Gudmundsson E. H., Pethick C. J., Epstein R. I., 1983, ApJ 272, 286
Güngör C., Güver T., Eksi K. Y., 2014, MNRAS, 439, 2717
Haensel P., Zdunik J. L., 1990, A&A, 227, 431
Haensel P., Kaminker A. D., Yakovlev D. G., 1996, A&A, 314, 328
Haensel P., Lasota J. P., Zdunik J. L., 1999, A&A, 344, 151
Haskell B., Patruno A., 2011, ApJ, 738, L14
Haskell B., Jones D. I., Andersson N., 2006, MNRAS, 373, 1423
Haskell B., Andersson N., Jones D. I., Samuelsson L., 2007, Phys. Rev. Lett., 99, 1101
Haskell B., Samuelsson L., Glampedakis K., Andersson N., 2008, MNRAS, 385, 531
Haskell B., Degenaar N., Ho W. C. G., 2012, MNRAS, 424, 93
Hild S., Chelkowski S., Freise A., 2008, preprint (arXiv:0810.0604)
Ho W. C. G., Andersson N., Haskell B., 2011, Phys. Rev. Lett., 107, 101101
Horowitz C. J., Kadau K., 2009, Phys. Rev. Lett., 103, 191102
Jahoda K., Markwardt C. B., Radeva Y., Rots A. H., Stark M. J., Swank J. H., Strohmayer T. E., Zhang W., 2006, ApJS 163, 401
Johnson-McDaniel N. K., Owen B. J., 2013, Phys. Rev. D, 88, 044004
Kalberla P. M. W., Burton W. B., Hartmann D., Arnal E. M., Bajaja E., Morras R., Pöppel W. G. L., 2005, A&A, 440, 775
Kobyakov D., Pethick C. J., 2014, Phys. Rev. Lett., 112, 112504
Konar S., Bhattacharya D., 1997, MNRAS, 284, 311
Konar S., Bhattacharya D., 1999, MNRAS, 303, 588
Krimm H. A. et al., 2007, ApJ, 668, L147
Lorenz C. P., Ravenhall D. G., Pethick C. J., 1993, Phys. Rev. Lett., 70, 379
Mahmoodifar S., Strohmayer T., 2013, ApJ, 773, 140
Maxwell O. V., 1979, ApJ, 231, 201
Melatos A., Payne D. J. B., 2005, ApJ, 623, 1044
Miller J. M. et al., 2003, ApJ, 583, L99
Misanovic Z., Galloway D. K., Cooper R. L., 2010, ApJ, 719, 947

Mukherjee D., Bhattacharya D, 2012, MNRAS, 420, 720
Mukherjee D., Bhattacharya D., Mignone A., 2013a, MNRAS, 430, 1976
Mukherjee D., Bhattacharya D., Mignone A., 2013b, MNRAS, 435, 718
Narita T., Grindlay J. E., Barret D., 2001, ApJ, 547, 420
Owen B. J., 1995, Phys. Rev. Lett., 95, 211101
Papaloizou J., Pringle J. E., 1978, MNRAS, 184, 501
Papitto A. et al., 2013a, MNRAS, 329, 3411
Papitto A. et al., 2013b, Nature, 501, 517
Patruno A., 2010, ApJ, 722, 909
Patruno A., Watts A. L., 2012, in Belloni T., Mendez M., Zhang C. M., eds, Timing neutron stars: pulsations, oscillations and explosions, Accreting Millisecond X-Ray Pulsars. Astrophys. Space Sci. Libr., Springer-Verlag, Berlin, preprint (arXiv:1206.2727)
Patruno A., Rea N., Altamirano D., Linares M., Wijnands R., van der Klis M., 2009, MNRAS, 396, L51
Patruno A., Haskell B., D'Angelo C.20122012, ApJ, 746, 9
Payne D. J. B., Melatos A., 2004, MNRAS, 351, 569
Piraino S., Santangelo A., Ford E. C., Kaaret P., 1999, A&A, 349, L77
Priymak M., Melatos A., Payne D. J. B., 2011, MNRAS, 417, 2696
Priymak M., Melatos A., Lasky P. D., 2014, MNRAS, 445, 2710
Radhakrishnan V., Srinivasan G., 1982, Curr. Sci, 51, 1096
Riles K., 2013, Prog. Part. Nucl. Phys., 68, 1
Schatz H. et al., 2014, Nature, 505, 62
Shibazaki N., Murakami T., Shaham J., Nomoto K., 1989, Nature, 342, 656
Ushomirsky G., Rutledge R. E., 2001, MNRAS, 325, 1157
Ushomirsky G., Cutler C., Bildsten L., 2000, MNRAS, 319, 902
van Straaten S., van der Kils M., Mendez M., 2003, ApJ, 596, 1155
Vigelius M., Melatos A., 2009a, MNRAS, 395, 1972
Vigelius M., Melatos A., 2009b, MNRAS, 395, 1985
Wagoner R. V., 1984, ApJ, 278, 345
Watts A. L., Krishnan B., Bildsten L., Schutz B. F., 2008, MNRAS, 389, 839
Wette K., Vigelius M., Melatos A., 2010, MNRAS, 402, 1099
White N., Zhang W., 1997, ApJ, 490, L87
Wijnand R., Degenaar N., Page D., 2013, MNRAS, 432, 2366

This paper has been typeset from a TEX/LATEX file prepared by the author.